scientific reports

Check for updates

OPEN

Contribution of non-linear internal waves to marine net primary production has been underestimated

Xiaoju Pan[1]✉, Tung-Yuan Ho[2], George T. F. Wong[2,3], Jen-Hua Tai[2], Shoude Guan[4] & Fuh-Kuo Shiah[2]

Field observations in the northern South China Sea (NSCS) indicate that elevated concentrations of chlorophyll a (Chl_a) associated with non-linear internal waves (NIWs) were more pronounced in the subsurface than at the sea-surface. At a given surface Chl_a, the vertically integrated Chl_a in an NIW-active area was 45% higher than that in an area where the NIW activities were minimal. As a result, net primary production (PP_{eu}) estimated from surface Chl_a from remote sensing by using the current Chl_a-based PP_{eu} model (e.g. VGPM) would have underestimated the true value by the same amount. If this correction is applied, the activities of NIWs would have elevated PP_{eu} in the NSCS by 89%, rather than by 15–37% as previously reported. The elevated PP_{eu} in the areas with high NIW activities would be at least 3.57 Tg-C yr^{-1}. It may account for 2.0% of new production in the South China Sea.

Marine net primary production (PP_{eu}) is a primary determining factor of the life processes in the oceans. It also plays a critical role in regulating atmospheric CO_2 which is a major contributing factor to global warming. Thus, an accurate quantification of PP_{eu} would be indispensable for a better understanding of these important processes in the earth system. Global marine PP_{eu}, at about 50 Pg-C yr^{-1}, is similar in magnitude to primary production on land, and it has been estimated to be decreasing at about 0.19 Pg-C or 0.4% per year[1,2]. This decrease has been postulated to be probably the result of global warming which may lead to an increase in the vertical stratification in the oceans, and a decrease in deep water formation. The resulting reduction in vertical mixing reduces the supply of nutrients from the nutrient-rich deep water to the nutrient-depleted surface water to support primary production. Within the oceans, higher PP_{eu} has been found in sub-regions where the activities of non-linear internal waves (NIWs; also called internal solitary waves) are prominent since these activities enhance vertical mixing[3,4]. These sub-regions in the oceans are quite ubiquitous[5] and they contribute disproportionately to global PP_{eu}. Pan et al.[6] estimated that the activities of NIWs may have elevated PP_{eu} by 15–37% in the northern South China Sea. Furthermore, under global warming, DeCarlo et al.[7] suggested that the activities of NIWs may intensify as vertical stratification increases. Thus, while global PP_{eu} may decrease, PP_{eu} in the sub-regions with NIW activities may increase so that its contribution to global PP_{eu} may be further amplified.

Regional and global PP_{eu} has been estimated almost exclusively from ocean color remote sensing[8]. A widely used, if not the most widely used, ocean color model is the Vertically Generalized Production Model (VGPM)[9] such that:

$$PPeu = 0.66125 \times P_{opt}^{B} \times \frac{E_0}{E_0 + 4.1} \times EZD \times C_s \times D_{irr} \quad (1)$$

Here, P_{opt}^{B}, E_0, EZD, C_s and D_{irr} represent the maximum carbon fixation rate within a water column, the daily integrated surface photosynthetically available radiation (PAR), the euphotic zonal depth, surface chlorophyll a concentration (Chl_a) and the daily photoperiod, respectively. P_{opt}^{B} can be expressed as a 7th -order polynomial function of sea surface temperature (SST), while (EZD×C_s) is actually a measure to the integrated chlorophyll in the euphotic zone (I_{Chl})[9]. Therefore, given the surface condition (e.g. SST and E_0, which are also readily available

[1]Yazhou Bay Innovation Institute/College of Marine Science and Technology/Key Laboratory for Coastal Marine Eco-Environment Process and Carbon Sink of Hainan Province, Hainan Tropical Ocean University, Sanya, Hainan, China. [2]Research Center for Environmental Changes, Academia Sinica, Taipei, Taiwan. [3]Department of Ocean, Earth and Atmospheric Sciences, Old Dominion University, Norfolk, VA, USA. [4]Physical Oceanography Laboratory, Ocean University of China, Qingdao, Shandong, China. ✉email: xiaojupan@hntou.edu.cn; xiaojupan@hotmail.com

satellite products), the VGPM-derived PP_{eu} is actually linearly related to I_{Chl}. In other words, quantifying I_{Chl} is key to the accurate estimation of PP_{eu} from space.

The I_{Chl} is estimated from surface Chl_a by using empirical relationships between the two[10]. An error may appear when this approach is used for estimating I_{Chl} in the sub-regions in the oceans where NIW is active, since the relationship between the subsurface distribution of Chl_a and surface Chl_a in the sub-regions with NIW activities[3,4,6] may differ from that in the general ocean on which the VGPM is based. Thus, the algorithms in use presently for the estimation of I_{Chl} and PP_{eu} may not yield accurate estimations of actual I_{Chl} and PP_{eu} in these sub-regions. Extensive activities of NIWs are known to occur in the norther South China Sea (NSCS)[11,12]. Generated at the Luzon Strait, theses NIWs propagate westward across the deep basin and evaluate according to bumpy topography, interaction with the oceanic circulations, and interaction with meso-scale eddies[13–16]. The NIWs become unsteady and dissipative as they propagate up the continental slopes. By using in situ and remotely sensed data from this sub-region, the potential error on the estimation of I_{Chl} in this type of environment and how it may affect the estimation of regional PP_{eu} are evaluated.

Materials and methods

Field experiments

The study area, 114.5–120.5° E and 19.5–22.0° N, in the open NSCS is an area where extensive activities of NIWs, based on satellite observations reported in literature, have been found (Fig. 1)[6,12]. Although the NIWs may occur in other parts of the NSCS, e.g. in the northwestn South China Sea (around 112–114 ° E and 19.5–22.0° N)[17], the area of these regions is one order of magnitude smaller than our study area. As such, the contribution of PP_{eu} by the NIWs in other sub-regions would be substantially limited as compared to that in our study area. In this area, the activities of NIWs are particularly intense around the Dongsha Atoll (116.68–116.92° E and 20.58–20.78° N). The NIWs are thought to be transformed and even dissipated north of the Dongsha Atoll, while east and south of the Dongsha Atoll are the transmission zones to the NIWs[6]. Waters with water-depths of less than 200 m were excluded from the analysis so as to minimize any influence from land runoff. Furthermore, in order to focus on the effect of the NIW alone, observations that might have been affected by episodes of tropical cyclones and eddies were also excluded. As the effect of the NIW in the upper layer tends to be masked when the waters are well mixed[6], only stations with vertically stratified waters were selected for analysis. A total of 10 stations in the study area were occupied in 6 cruises between 2009 and 2014 (Fig. 1; Table 1). At 5 stations, 3 occupied north and 2 occupied east of the Dongsha Atoll, time-series observations in 1 to 3-hour time-intervals were conducted for a time period of 20 to 38 h. During these time series observations, the activities of NIWs were indicated by oscillating isopycnals with depth at amplitudes of 43 ± 14 m (ranging between 29 and 64 m) and period of about 12 h (Fig. S1). Nevertheless, since the NIW passages occur in several to tens of minutes, higher temporal resolutions on the CTD profiles may help to capture the performance of the NIWs in more details.

The observations at the SouthEast Asian Time-series Study (SEATS) station (at 116° E, 18° N) in the deep basin of the NSCS were used as a reference as this station is located only about 150 km from the study area and the activities of NIWs at this location have known to be limited (Fig. 1)[6,12]. Over 400 km away from the coastline and with ~ 3800 m of water bottom depth, land effects, such as coastal upwelling and sediment resuspension,

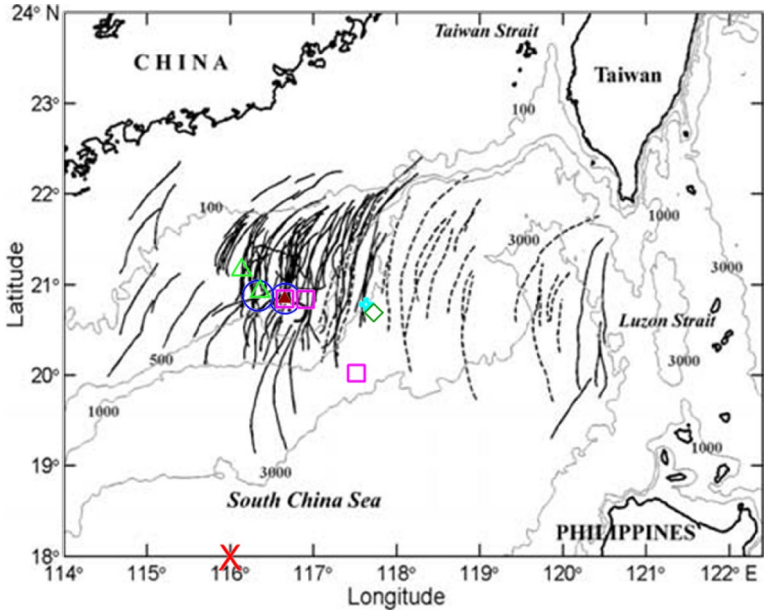

Fig. 1. Station locations in the northern South China Sea (NSCS). X: SEATS; ○: OR3-1379; □: OR1-0929; +: OR1-1015; ▲: OR3-1697; ◊: OR3-1770; Δ: OR1-1084. The historical compilation of the distribution of internal waves in the NSCS between 1995 and 2001 reported by Zhao et al.[12] is shown as the background.

Cruises	Periods	*Stations
(a) Stations with NIW effect		
OR3_1379	11–12 Jun 2009	2 (1)
OR1_0929	4–12 Jun 2010	3 (1)
OR1_1015	13–14 Oct 2012	1 (1)
OR3_1697	19–20 Jun 2013	1 (1)
OR3_1770	6–7 Jun 2014	1 (1)
OR1_1084	9–11 Aug 2014	2 (0)
(b) The SEATS station with minimal effect of the NIWs		
SEATS	19 Sep 1999; 23–24 May, 25–26 Jul 2000; 25–27 Mar 2002; 7 Aug, 4 Oct 2003; 5 May, 6 Aug 2004; 30 Mar, 30 Jul 2005; 21 Oct 2006; 31 May 2008; 14 Oct 2010; 31 Aug-1 Sep 2012; 16 Oct 2013; 5–6 Aug 2014	16 (16)

Table 1. Field experiments conducted in the open NSCS. *Number of stations in which number of the anchored stations is shown in parenthesis.

are almost negligible at the SEATS station. Similar to the observations in the NIW-active area, observations at the SEATS station that might have been affected by episodes of tropical cyclones and eddies were also excluded. The SEATS station was occupied 16 times between 1999 and 2014, and time-series observations in 1 to 3-hour time-intervals were conducted for a time period of 9 to 44 h. In these observations, regular oscillations of the isopycnals with depth were not found consistently (Fig. S2). If oscillations were found, the amplitudes were 14 ± 6 m (ranging between 4 and 26 m). Thus, the activities of NIWs were small in comparison to those at the study area during the study period.

Each time when a station was occupied, the distributions of water temperature and salinity were recorded with depth with a conductivity-temperature-depth (CTD) recorder (SeaBird SBE9/11), while photosynthetically available radiation (PAR) and in situ chlorophyll fluorescence were measured by a Biospherical model QSP-200 L or QSR-240 quantum scalar irradiance sensor and a Chelsea AQUAtracka III fluorometer, respectively. These vertical observations were binned to 1-m intervals. The mixed layer depth (MLD) is defined as the depth at which the temperature was 0.5 °C lower than the surface value, while the euphotic zonal depth (EZD) is defined here as the depth at which PAR was reduced to 0.6% of the surface value[18]. The subsurface chlorophyll maximum depth is determined as the depth with the maximum chlorophyll fluorescence. The dissipation rate of turbulent kinetic energy (ε) and eddy diffusivity (K_p) are estimated using the Thorpe scale method such that[19]:

$$\varepsilon \approx 0.64 {L_T}^2 N^3 \tag{2}$$

$$K_p \approx 0.2\varepsilon / N^2 \tag{3}$$

Here, the Thorpe scale (L_T) is estimated by following the method described in Dillon[20] and Thorpe[21], while the Brunt-Väisälä frequency (N) is estimated as:

$$\mathrm{N} = \sqrt{\frac{g}{\rho} d\rho / dz} \tag{4}$$

Here, g is the acceleration due to gravity (≈9.8 m s^{-2}), ρ is the density, and z is the depth.

Discrete water samples were collected at 6 to 9 depths in the top 200 m of the water column, typically at nominal depths of 5, 10, 20, 30, 50, 80, 100, 150 and 200 m, by using 20-L Go-Flo bottles mounted onto a Rosette sampling assembly (General Oceanic Inc.). Samples for the determination of the Chl_a were collected by filtering ~ 2-L of seawater each onboard ship through 47 mm Whatman GF/F glass fiber filters. The filters were stored in liquid nitrogen and were returned to shore-based laboratories for the determination of the concentrations of Chl_a by fluorimetry prior to 2007 and by high-performance liquid chromatography (HPLC) in subsequent years[22,23]. The column-integrated Chl_a utilized for photosynthesis, I_{Chl}, was calculated by trapezoidal integration for the euphotic zone. To reduce the error in the calculation of I_{Chl} when the subsurface Chl_a maximum depth, which was typically located at ~ 60 m, was not sampled, the concentrations of Chl_a below 50 m in 1-m intervals were estimated from the in situ chlorophyll fluorescence. For each cast, an empirical linear relationship, which was regressed from the match-up data points between discrete water samples and the corresponding in situ chlorophyll fluorescence below 50 m, was used to convert the in situ fluorescence to the concentrations of Chl_a.

Remotely sensed data

Monthly VGPM-derived PP_{eu} obtained with the MODerate resolution Imaging Spectroradiometer on Aqua sensor (MODIS-Aqua) between 2002 and 2024 was extracted from the Ocean Productivity site (http://www.science.oregonstate.edu/ocean.productivity/index.php).

Statistics

The performance of the algorithm of the derivations was evaluated by the root mean square difference (RMSD) such that:

$$\mathrm{RMSD}=\sqrt{\sum (\mathrm{D}-\mathrm{F})2/\mathrm{n}} \quad (5)$$

Here, n, F and D are the number of samples, the observations and the corresponding derived products, respectively.

Results and discussion

Effect of the NIWs on enhancing subsurface Chl_a

The vertical distributions of Chl_a in the summer at the SEATS station on 5–6 August 2014 and in the study area at Station A (north of the Dongsha Atoll at 116.66° E, 20.85° N) on 8–10 June 2010 are shown in Fig. 2. The observations at these two stations are approximately representative of the average summer conditions at the SEATS station and in the NIW-active sub-region, respectively (Table S1). The hydrographic conditions, such as sea surface temperature (SST; 29.2 ± 0.1 vs. 28.0 ± 0.1 °C), MLD (24 ± 3 vs. 32 ± 9 m) and EZD (77 ± 5 vs. 74 ± 6 m), were not substantially different to each other at these two stations. As such, the difference between these two stations might indicate the general response of phytoplankton to the NIWs.

At the SEATS station, the low surface Chl_a, 0.13 ± 0.02 mg m^{-3}, was typically observed in the open NSCS in the summer when the mixed layer waters were relatively oligotrophic[23]. Below the mixed layer, Chl_a increased with increasing depth until a maximum of 0.33 mg m^{-3} was reached at the subsurface chlorophyll maximum (SCM). Below the maximum, the concentration decreased sharply with depth as light became limiting for phytoplankton growth, and reached undetectable levels below about 150 m. Such a depth distribution in Chl_a and the concentration of Chl_a at the subsurface are typical of what have been observed at this station over the years[24] and have been found in many parts of the oceans, especially in tropical waters[25]. At Station A, the surface Chl_a, 0.10 ± 0.02mg m^{-3}, was similar to those at the SEATS station and was typical of those found in the open NSCS in the summer[23]. However, although the vertical distribution of Chl_a at Station A followed a similar pattern as that at the SEATS station, prominently elevated concentrations were found around the subsurface maximum from the base of the mixed layer (at ~ 30 m) to ~ 100 m. In this Chl_a-rich layer, the average ratio of Chl_a to the surface value was about 3.3 ± 1.2 (ranging between 1.1 and 5.1) at Station A. The corresponding value at the SEATS station was 1.8 ± 0.5 (ranging between 0.9 and 2.5). Thus, while the surface Chl_a at Station A, 0.10 ± 0.02mg m^{-3}, was lower, by about 30%, than that, 0.13 ± 0.02 mg m^{-3}, at the SEATS station, the column-integrated Chl_a utilized for photosynthesis, I_{Chl}, at Station A (21.4 ± 3.1 mg m^{-2}) was higher, by about 15%, than that at the SEATS station (18.5 ± 2.4 mg m^{-2}). In other words, I_{Chl} was significantly elevated at the station where the activities of NIWs were extensive and this elevation was not reflected in surface Chl_a.

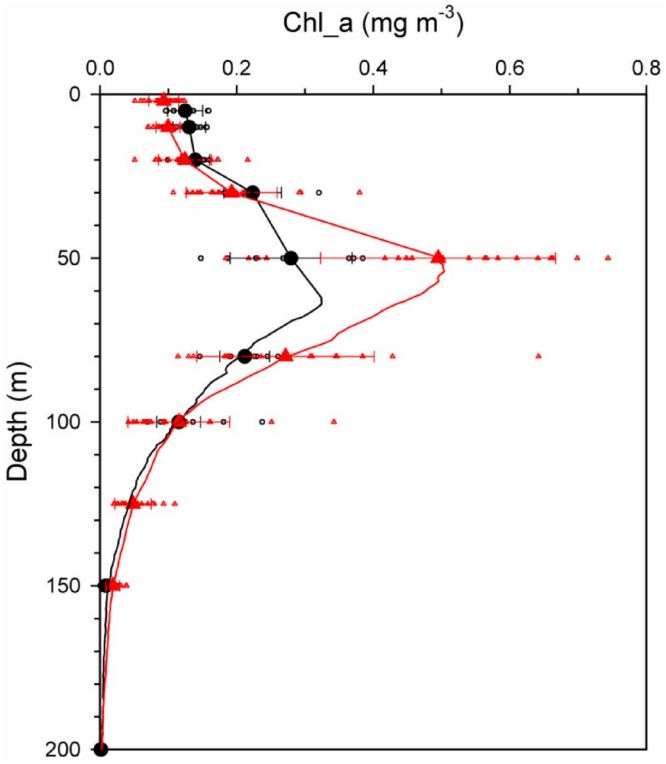

Fig. 2. Average vertical variations of Chl_a (solid lines) at the SEATS station (●) conducted during 5–6 August 2014 and at the Station A (▲) conducted during 8–10 June 2010. Small-sized symbols – individual observations from discrete water sampling; large-sized symbols and error bars – mean ± SD of Chl_a from discrete water sampling. Note that Chl_a below 50 m was estimated from the in situ fluorescence with 1-m intervals.

Three effects of the NIWs might contribute to the relative elevation of subsurface Chl_a at Station A. First, the SCM was elevated to shallower depth, and also optically shallower depth, by the NIWs. It was located at ~ 54 m or ~ 3.0% of the surface PAR at Station A, shallower than that, ~ 64 m or ~ 1.6%, at the SEATS station. Secondly and probably more importantly, the vertical mixing would be enhanced by the NIWs. The average eddy diffusivity (K_p) in the subsurface layer (e.g. depth of 50–100 m) at Station A, 0.00023 ± 0.00100 $m^2\ s^{-1}$ (ranging between 0 and 0.00616 $m^2\ s^{-1}$), was about 2.3-folds of that at the SEATS station, 0.00010 ± 0.00030 $m^2\ s^{-1}$ (ranging between 0 and 0.00099 $m^2\ s^{-1}$). Similar results were found in other stations. For example, the average K_p in the anchored stations in the NIW-active sub-region, 0.00038 ± 0.00060 $m^2\ s^{-1}$ (ranging between 0.00001 and 0.00143 $m^2\ s^{-1}$), was 4.6-folds of the average K_p at all observations at the SEATS station, 0.00008 ± 0.00011 $m^2\ s^{-1}$ (ranging between 0.0 and 0.00034 $m^2\ s^{-1}$). As such, the elevated nutrient supply from the nutrient-rich lower waters by the NIWs would support elevated phytoplankton growth in the euphotic zone. Thirdly, on the continental slopes, the formation of NIWs with subsurface trapped cores via shoaling makes the waters highly turbulent with 10–50-m density overturnings[26,27]. The cores mix continuously with the surronding waters and create wakes of mixed waters.

Relationships between I_{Chl} and surface Chl_a observed in situ

At the SEATS station, the field in situ observations indicated that I_{Chl} generally increased with the increase of surface Chl_a, C_s, and the relationship between them could be expressed as a log-transformed linear (Model-2) regression such that (Fig. 3):

$$\log(\mathrm{IChl})\,\mathrm{ref} = (1.784 \pm 0.047) + (0.567 \pm 0.050)\log(\mathrm{Cs})\,\mathrm{ref}$$
$$r^2 = 0.734,\ n = 46 \quad (6)$$

Here, the subscript "ref" represents the reference site at the SEATS station. The RMSD of $\log(I_{Chl})_{ref}$ derived from Eq. (5) relative to the in situ observations was ± 0.0415, which was corresponding to the uncertainty of the derived $(I_{Chl})_{ref}$ by about ± 10%.

For stations associated with the NIWs, I_{Chl} could also be related to C_s by a log-transformed linear (Model-2) regression such that (Fig. 3):

$$\log(\mathrm{IChl})\,\mathrm{NIW} = (1.969 \pm 0.058) + (0.600 \pm 0.057)\log(\mathrm{Cs})\,\mathrm{NIW}$$
$$r^2 = 0.687,\ n = 51 \quad (7)$$

Here, the subscript "NIW" represents the region subject to the effect of the NIWs. The RMSD of the derived $\log(I_{Chl})_{NIW}$ relative to the in situ observations was ± 0.0906, which was corresponding to the uncertainty of the derived $(I_{Chl})_{NIW}$ by about ± 23%. Although the influence of NIW activities on the vertical distributions of Chl_a may be spatially different due to spatial variability in wave energy, bathymetry, hydrography and so on,

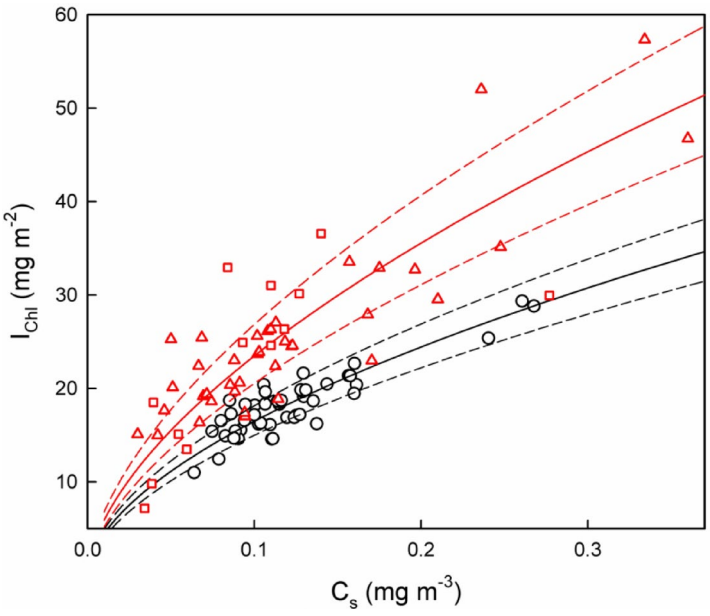

Fig. 3. Relationships between column-integrated Chl_a utilized for photosynthesis (I_{Chl}) and surface Chl_a (C_s) from field in situ observations. ○: SEATS station; △, □: Stations subject to the effect of the NIWs with water bottom depths of ~ 350 m and > 1000 m, respectively. Solid lines – best fit log-transformed linear regressions; dashed lines – one RMSD (± 0.0415 and ± 0.0906) of $\log(I_{Chl})$ from the best fit lines at the SEATS station and stations associated with the NIWs, respectively.

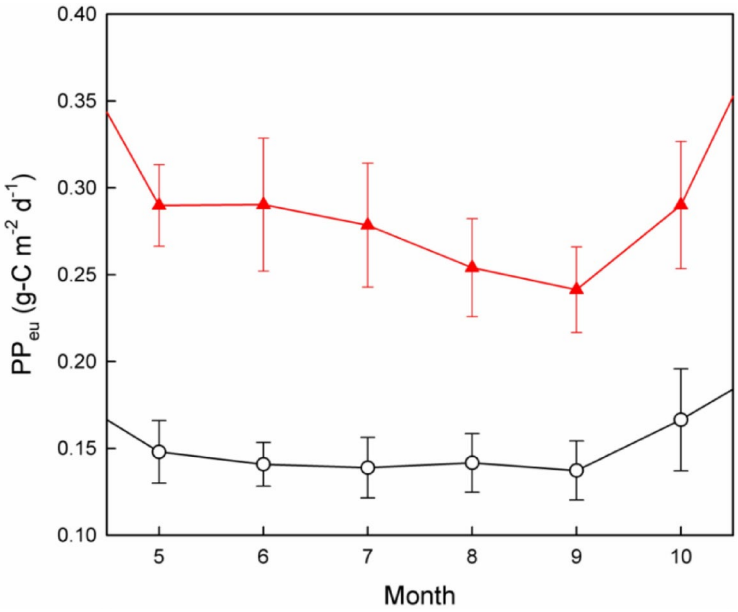

Fig. 4. "Corrected" MODIS-Aqua derived climatological (2002–2024) monthly mean ± SD of net primary production (PP_{eu}) between May and October. ○: at the SEATS station; ▲: in the NIW-active sub-region (114.5–120.5.5.5° E and 19.5–22.0° N).

the relationships between I_{Chl} and C_s were not substantially spatially different. For examples, when separating stations into two groups, one with water bottom depths of ~ 350 m in representing the regions where the NIWs are transformed or even dissipated, and the other with water bottom depths > 1000 m in representing the transmission zones for the NIWs, the relationships between by $(I_{Chl})_{NIW}$ and $(C_s)_{NIW}$ were not substantially different to each other (Fig. 3). As such, Eq. (7) would be relatively uniform for NIW-active regions.

For a given C_s, $(I_{Chl})_{NIW}$ was generally larger than $(I_{Chl})_{ref}$ (Fig. 3). Since the slopes in Eqs. (6) and (7), 0.567 and 0.600 respectively, were not substantially different to each other, the ratio of $(I_{Chl})_{NIW}$ to $(I_{Chl})_{ref}$ was largely independent of C_s and was thus approximately a constant. Actually, for C_s ranging between 0.05 and 0.35 mg m^{-3}, which may cover most of the surface Chl_a observed in the stratified waters of the open NSCS[23], the ratio of $(I_{Chl})_{NIW}$ to $(I_{Chl})_{ref}$ was about 1.45 (varying between 1.39 and 1.48). In other words, at a given C_s, I_{Chl} in the region with extensive activities of NIWs was about 45% higher than that in a region where the activities of NIW was minimal.

Impacts to regional and global carbon cycles

At the SEATS station, Shih et al[28]. indicated that between April and October, the "true" PP_{eu} obtained from the ship-based in situ measurements would be about 0.64-fold of the satellite-derived VGPM-based PP_{eu}. In the NIW-active sub-region, as the VGPM-based PP_{eu} is actually linearly related to I_{Chl}, according to the results in Sect. 3.2, the "true" PP_{eu} would be about 0.928-fold (1.45 × 0.64 = 0.928) of the satellite-derived VGPM-based PP_{eu}. Figure 4 showed the climatological monthly PP_{eu} corrected by multiplying 0.64 and 0.928 to the MODIS-derived VGPM-based net primary production at the SEATS station and in the NIW-active region (114.5–120.5.5.5° E and 19.5–22.0° N), respectively, between May and October when the effects of the NIWs are marked[6,23].

In the NIW-active sub-region, the PP_{eu} between May and October was about 0.274 ± 0.021 g-C m^{-2} d^{-1} (ranging between 0.241 and 0.290 g-C m^{-2} d^{-1}). Compared to the PP_{eu}, 0.146 ± 0.018 g-C m^{-2} d^{-1} (ranging between 0.137 and 0.166 g-C m^{-2} d^{-1}), at the SEATS station during the same time period, the PP_{eu} would be elevated by 89% associated with the NIW activities, rather than 15–37% in previous report[6]. The contribution of the NIWs on enhancing PP_{eu} would reach 0.128 g-C m^{-2} d^{-1}. It was equal to 3.57 × 10^{12} g-C yr^{-1} or 3.57 Tg-C yr^{-1} (1 Tg = 10^{12} g), given the NIW-active sub-region covering an area of 0.15 × 10^6 km^2 in a time period of 183 days (May to October). Such a contribution is about 1.1-fold of that, 3.27 Tg-C yr^{-1}, caused by the tropical cyclones in the whole western North Pacific subtropical ocean[29]. Given that the NIWs may occur in other parts of the SCS, although their area is substantially small as compared to our selected study area, the enhanced PP_{eu} contributed by the NIW activities would be slightly larger than our estimation.

The PP_{eu} enhanced by the NIWs is attributed to the new production. The new production in the South China Sea (SCS) was about 0.14 g-C m^{-2} d^{-1} year round[30]. Covering an area of 3.5 × 10^6 km^2, the annual new production in the SCS as a whole would reach 179 Tg-C yr^{-1}. Therefore, even without considering the contributions from other regions in the SCS, the NIWs might contribute about 2.0% (= 3.57/179) of the new production in the SCS. Since the NIWs are commonly found in the shelf-seas[5], the global contribution of the new production by the NIWs, as well as the contribution to the global anthropogenic CO_2 uptake, would need to be re-evaluated.

Conclusion

This study has demonstrated that the subsurface Chl_a in the sub-region subject to the effect of the NIWs would be pronouncedly higher than that in the sub-region with minimal effect of the NIWs in the NSCS. As such, for a given surface Chl_a (C_s), the vertically integrated Chl_a (I_{Chl}) in the NIW-active sub-region would be higher by 45% than that in the general condition. Current Chl_a-based remote sensing primary production model (e.g. VGPM), which adapts the relationship between I_{Chl} and C_s developed for the general condition, would underestimate net primary production (PP_{eu}) in the NIW-active sub-region. By using the corrected data, the NIWs would cause an elevation of PP_{eu} by about 89%, rather than 15–37% previously reported[6]. The elevated PP_{eu} associated with the NIWs would be at least 3.57 Tg-C yr^{-1} in the South China Sea (SCS). The NIWs may account for 2.0% of new production in the SCS. Nevertheless, since only 10 stations are available for the NIW-active region, further evaluation when additional field observations, which cover broader geographic scope, become available would be desirable.

Data availability

The datasets generated during the current study are available in the Figshare repository, doi: 10.6084/m9.figshare.31819483.

Received: 18 November 2025; Accepted: 17 March 2026
Published online: 22 March 2026

References

1. Behrenfeld, M. J. et al. Climate-driven trends in contemporary ocean productivity. *Nature* **444**, 752–755 (2006).
2. Chavez, F. P., Messié, M. & Pennington, J. T. Marine primary production in relation to climate variability and change. *Annu. Rev. Mar. Sci.* **3**, 227–60 (2011).
3. da Silva, J. C. B., New, A. L., Srokosz, M. A. & Smyth, T. J. On the observability of internal tidal waves in remotely-sensed ocean colour data. *Geophys. Res. Lett.* **29**(12), 1569 (2002).
4. Wang, Y. H., Dai, C. F. & Chen, Y. Y. Physical and ecological processes of internal waves on an isolated reef ecosystem in the South China Sea. *Geophys. Res. Lett.* **34**, L18609 (2007).
5. Woodson, C. B. The fate and impact of internal waves in nearshore ecosystems. *Annu. Rev. Mar. Sci.* **10**, 421–441 (2018).
6. Pan, X., Wong, G. T. F., Shiah, F. K. & Ho, T. Y. Enhancement of biological productivity by internal waves: Observations in the summertime in the northern South China Sea. *J. Oceanogr.* **68**, 427–437 (2012).
7. DeCarlo, T. M., Karnauskas, K. B., Davis, K. A. & Wong, G. T. F. Climate modulates internal wave activity in the Northern South China Sea. *Geophys. Res. Lett.* **42**, 831–838 (2015).
8. McClain, C. R. A decade of satellite ocean color observations. *Annu. Rev. Mar. Sci.* **1**, 19–42 (2009).
9. Behrenfeld, M. J. & Falkowski, P. G. Photosynthetic rates derived from satellite-based chlorophyll concentration. *Limnol. Oceanogr.* **42**(1), 1–20 (1997).
10. Morel, A. & Berthon, J. F. Surface pigments, algal biomass profiles, and potential production of the euphotic layer: Relationships reinvestigated in view of remote-sensing applications. *Limnol. Oceanogr.* **34**, 1545–1562 (1989).
11. Liu, C. T. et al. Nonlinear internal waves from the Luzon Strait. *Eos Transaction AGU* **87**(42), 449–451 (2006).
12. Zhao, Z., Klemas, V., Zheng, Q. & Yan, X. H. Remote sensing evidence for baroclinic tide origin of internal solitary waves in the Northeastern South China Sea. *Geophys. Res. Lett.* **31**, L06302 (2004).
13. Xie, J. et al. Variation of internal solitary wave propagation induced by the typical oceanic circulation patterns in the Northern South China Sea deep basin. *Geophys. Res. Lett.* **48**, e2021GL093969 (2021).
14. Xie, J., He, Y. & Cai, S. Bumpy topographic effects on the transbasin evolution of large-amplitude internal solitary wave in the Northern South China Sea. *J. Geophys. Research: Oceans* **124**, 4677–4695 (2019).
15. Xie, J. et al. Distortion and broadening of internal solitary wavefront in the Northeastern South China Sea deep basin. *Geophys. Res. Lett.* **43**, 7617–7624 (2016).
16. Xie, J., He, Y., Chen, Z., Xu, J. & Cai, S. Simulations of internal solitary wave interactions with mesoscale eddies in the Northeastern South China Sea. *J. Phys. Oceanogr.* **45**, 2959–2978 (2015).
17. Li, X., Zhao, Z. & Pichel, W. G. Internal solitary waves in the northwestern South China Sea inferred from satellite images. *Geophys. Res. Lett.* **35**, L13605 (2008).
18. Chen, Y. L. & Chen, H. Y. Seasonal dynamics of primary and new production in the northern South China Sea: The significance of river discharge and nutrient advection. *Deep Sea Res. Part I Oceanogr. Res. Pap.* **53**, 971–9 (2006).
19. Osborn, T. R. Estimates of the local rate of vertical diffusion from dissipation measurements. *J. Phys. Oceanogr.* **10**, 83–89 (1980).
20. Dillon, T. M. Vertical overturns: A comparison of Thorpe and Ozmidov length scales. *J. Geophys. Res.* **87**(C12), 9601–9613 (1982).
21. Thorpe, S. A. Turbulence and mixing in a Scottish loch. *Philos. Trans. R. Soc. Lond. A* **286**, 125–181 (1977).
22. Ho, T. Y., Pan, X., Yang, H. H., Wong, G. T. F. & Shiah, F. K. Controls on temporal and spatial variations of phytoplankton pigment distribution in the northern South China Sea. *Deep Sea Res. Part II Top. Stud. Oceanogr.* **117**, 65–85 (2015).
23. Pan, X., Wong, G. T. F., Tai, J. H. & Ho, T. Y. Climatology of physical hydrographic and biological characteristics of the northern South China Sea Shelf-sea (NoSoCS) and adjacent waters: Observations from satellite remote sensing. *Deep Sea Res. Part II Top. Stud. Oceanogr.* **117**, 10–22 (2015).
24. Liu, K. K. et al. The significance of phytoplankton photo-adaptation and benthic-pelagic coupling to primary production in the South China Sea: Observations and numerical investigations. *Deep Sea Res. Part II Top. Stud. Oceanogr.* **54**, 1546–1574 (2007).
25. Mann, K. H. & Lazier, J. R. N. *Dynamics of marine ecosystems: Biological-physical interactions in the oceans*. (Blackwell Science, 1996).
26. Lamb, K. G. A numerical investigation of solitary internal waves with trapped cores formed via shoaling. *J. Fluid Mech.* **451**, 109–144 (2002).
27. Lien, R. C. et al. Trapped core formation within a shoaling nonlinear internal wave. *J. Phys. Oceanogr.* **42**(4), 511–525 (2012).
28. Shih, Y. Y. et al. Comparison of primary production using in situ and satellite-derived values at the SEATS Station in the South China Sea. *Front. Mar. Sci.* **8**, 747763 (2021).
29. Lin, I. I. Typhoon-induced phytoplankton blooms and primary productivity increase in the western North Pacific subtropical ocean. *J. Geophys. Res.* **117**, C03039 (2012).
30. Chen, Y. L. Spatial and seasonal variations of nitrate-based new production and primary production in the South China Sea. *Deep Sea Res. Part I Oceanogr. Res. Pap.* **52**, 319–340 (2005).

Acknowledgements
The captain and the crews of R/V *Ocean Research-1* and R/V *Ocean Research-3* assisted in sample collection.

Author contributions
Conceptualization (XP, GW), methodology (XP, TH, GW, SG), software (XP, JT, SG), validation (XP, JT, SG, FS), formal analysis (XP, TH, JT), investigation (XP, TH, JT, FS), resources (XP, GW), data curation (XP, TH, GW, JT), writing—original draft preparation (XP, TH), writing—review and editing (XP, GW, SG, FS), visualization (JT, SG), supervision (XP, GW), project administration (XP), funding acquisition (XP). All authors have read and agreed to the published version of the manuscript.

Funding
This work was supported by National Natural Science Foundation of China (grant number 42266005), Major Science and Technology Program of Yazhou Bay Innovation Institute of Hainan Tropical Ocean University (grant numbers 2022CXYZD003, 2023CXYZD001) to XP, the Key Laboratory of Ocean Observation and Information of Hainan Province (grant number HKLOOI-OF-2023-01) to XP; Scientific Research Foundation of Hainan Tropical Ocean University (grant number RHDRC202103) to XP, and Special Program of Hainan Province for Academician Innovation Platform (grant number YSPTZX202507) to XP.

Declarations

Competing interests
The authors declare no competing interests.

Additional information
Supplementary Information The online version contains supplementary material available at https://doi.org/10.1038/s41598-026-45238-1.

Correspondence and requests for materials should be addressed to X.P.

Reprints and permissions information is available at www.nature.com/reprints.

Publisher's note Springer Nature remains neutral with regard to jurisdictional claims in published maps and institutional affiliations.